










# Molecular Gas and Star-formation in Low Surface Brightness Galaxies

Tian-Wen Cao<sup>1,2,3</sup> , Hong Wu<sup>1,2</sup>, Wei Du<sup>1</sup> , Feng-Jie Lei<sup>1,2</sup>, Ming Zhu<sup>1</sup>, Jan Wouterloot<sup>4</sup> , Harriet Parsons<sup>4</sup> ,  
Yi-Nan Zhu<sup>1</sup> , Chao-Jian Wu<sup>1</sup> , Fan Yang<sup>1</sup>, Chen Cao<sup>5</sup>, Zhi-Min Zhou<sup>1</sup> , Min He<sup>1,2</sup>, Jun-Jie Jin<sup>1,2</sup>, and James E. Wicker<sup>1</sup>

<sup>1</sup>Key Laboratory of Optical Astronomy, National Astronomical Observatories, Chinese Academy of Sciences, Beijing 100012, P.R. China; twcao@bao.ac.cn

<sup>2</sup>School of Astronomy and Space Science, University of Chinese Academy of Sciences, Beijing, P.R. China; hwu@bao.ac.cn

<sup>3</sup>Chinese Academy of Sciences South America Center for Astronomy, China-Chile Joint Center for Astronomy,  
Camino El Observatorio 1515, Las Condes, Santiago, Chile

<sup>4</sup>East Asian Observatory, 660 N. Aohōkū Place, University Park, Hilo, HI 96720, USA

<sup>5</sup>School of Space Science and Physics, Shandong University at Weihai, Weihai, Shandong 264209, China

Received 2017 April 15; revised 2017 July 23; accepted 2017 August 3; published 2017 August 30

## Abstract

We have obtained CO( $J = 2-1$ ) spectra of nine face-on low surface brightness galaxies using the JCMT 15 m telescope and observed H $\alpha$  images using the 2.16 m telescope of NAOC. As no CO has been detected, only upper limits on the H $_2$  masses are given. The upper limits of total molecular hydrogen masses are about  $(1.2-82.4) \times 10^7 M_\odot$ . Their star-formation rates are mainly lower than  $0.4 M_\odot \text{ yr}^{-1}$  and star-formation efficiencies are lower than  $1.364 \times 10^{-10} \text{ yr}^{-1}$ . Our results show that the absence of molecular gas content is the direct reason for the low star-formation rate. The low star-formation efficiency probably resulted from the low efficiency of H I gas transforming to H $_2$  gas.

*Key words:* galaxies: evolution – galaxies: star formation – ISM: molecules

## 1. Introduction

Low surface brightness galaxies (LSBGs, Impey & Bothun 1997) are important for investigating the evolution of our universe. The origin and evolution of these LSBGs are still mysterious. They have significantly different chemical enrichment histories from normal galaxies (Peebles 2001; Pustilnik et al. 2011). LSBGs are usually optically faint and blue (de Blok et al. 1995; Impey & Bothun 1997). The stellar disks of most LSBGs are diffuse. They usually have low metallicities ( $Z < 1/3 Z_\odot$ , McGaugh 1994), low column densities ( $N_{\text{HI}} \sim 10^{20} \text{ cm}^{-2}$ , de Blok et al. 1996), and low dust masses (Matthews & Wood 2001). The star-formation rates (SFRs) of LSBGs are lower than those of normal galaxies (Gerritsen & de Blok 1999; Boissier et al. 2008; Wyder et al. 2009).

According to previous works, the H I content of most LSBGs is rich, compared with normal star-forming (SF) galaxies (McGaugh 1994). The H I gas disk extends well beyond the stellar disk (McGaugh & de Blok 1997; Gerritsen & de Blok 1999; Matthews et al. 2001; O’Neil et al. 2004) and is about double the size of the optical disk (de Blok et al. 1996; Pickering et al. 1997; Das et al. 2007).

Although the original material involved in star formation is H I, the star formation is indirectly related to H I. Generally, the star formation arises out of molecular clouds. The low star-formation rates in LSBGs may be related to the absence of molecular gas content. The optical peculiarities of LSBGs have been discussed in some works (van der Hulst et al. 1993; McGaugh 1994; McGaugh & Bothun 1994; de Blok et al. 1995; Impey & Bothun 1997; Jimenez et al. 1998); however, the cold molecular gas in these galaxies is far from well understood. Molecular gas is vital for studying the star-formation process. There are some previous works that try to detect the CO content in LSBGs (Schombert et al. 1990; Knezek 1993; de Blok & van der Hulst 1998b; Braine et al. 2000). Most works just give upper limits on CO content, and only a few LSBGs have detected molecular gas (Matthews & Gao 2001; O’Neil et al. 2003; Matthews et al. 2005; Das et al.

2010; Haynes et al. 2011). This may indicate a shortage of molecular gas in LSBGs.

To explore the low star-formation efficiency (SFE) of LSBGs, we need to know which phase is dominant during star formation. There are two phases in the formation of a star: first, the H I gas transforms into molecular gas, then molecular gas forms a star. The CO( $J = 2-1$ ) emission line is used to trace molecular hydrogen gas in this work. We observe the CO ( $J = 2-1$ ) emission line by JCMT, H $\alpha$  images by the 2.16 m telescope of NAOC and also combine with NUV data from GALEX and H I data from Arecibo.

In this paper, the sample and observations of LSBGs are presented in Section 2. Results and an analysis are given in Section 3. Discussion and summary are provided in Section 4 and Section 5.

## 2. The Sample and Observation of LSBGs

### 2.1. Sample

The Arecibo Legacy Fast ALFA (ALFALFA) survey (Giovanelli et al. 2005), which covers  $7000 \text{ deg}^2$  of high Galactic latitude sky, provides a 21 cm H I emission line spectral database with redshifts from 1600 to  $18,000 \text{ km s}^{-1}$  and a velocity resolution of  $5 \text{ km s}^{-1}$ . The  $\alpha.40$  catalog is the first released catalog that covers 40% of the area of the ALFALFA survey and contains 15,855 objects (Haynes et al. 2011). About 78% of sources have optical counterparts from the Sloan Digital Sky Survey (SDSS, Haynes et al. 2011).

Based on the  $\alpha.40$  catalog, Du et al. (2015) selects a sample of LSBGs that contains 1129 LSBGs with surface brightnesses  $\mu_{\text{B}(0)\text{obs}}$  larger than  $22.5 \text{ mag arcsec}^{-2}$ . We selected nine LSBGs from this sample. They all have face-on disks and their H I masses are about  $(0.52-19.9) \times 10^9 M_\odot$ , and are expected to have higher fluxes of CO( $J = 2-1$ ) emission lines than others in the 1129 LSBGs sample. The redshifts in our sample are between 0.0029 and 0.0339. Generally, the size of the CO disk is about half the size of the optical disk (Young & Knezek 1989) and the optical sizes of nine targets are about

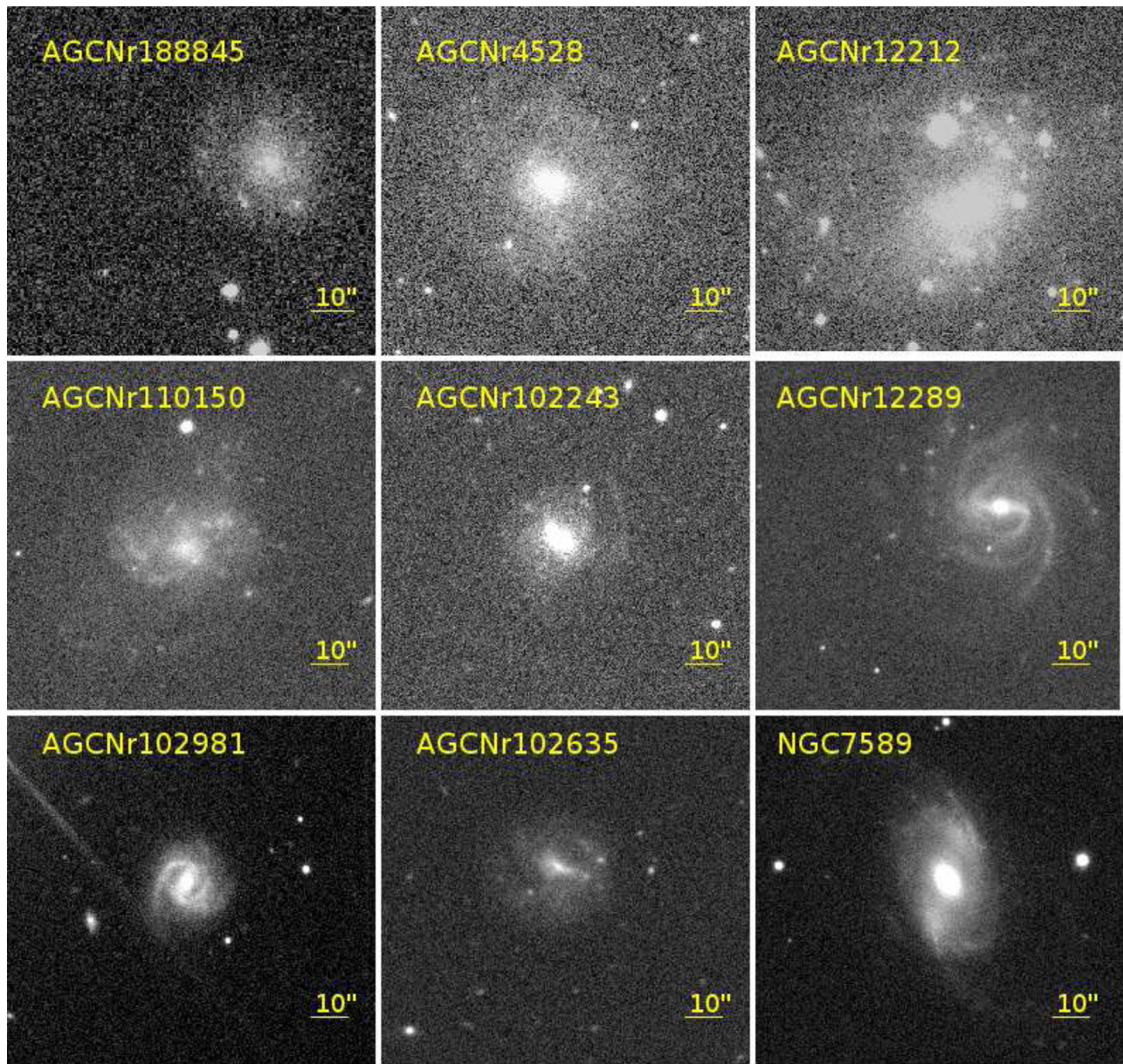


Figure 1. SDSS r-band images of our LSBGs.

30–80 arcsec. Figure 1 shows r-band images of our nine LSBGs from SDSS DR12. More details about properties of the galaxies are shown in Table 1.

### 2.2. $CO(J=2-1)$ Emission

We obtained  $CO(J=2-1)$  spectra of nine targets using the  $R \times A3$  receiver with ACSIS as the backend, mounted on the JCMT 15 m telescope near the peak of Mauna Kea, Hawaii. The half power beam width is about  $20''$  at 230 GHz. The frequency coverage of the A3 receiver ranges from 211.5 to 276.5 GHz and the  $CO(J=2-1)$  spectra of our objects shift from 222.99 to 229.86 GHz. The A3 receiver gives 1936 channels over a bandwidth of 1 GHz with a channel separation of 0.516 MHz, and the velocity resolution is  $0.674 \text{ km s}^{-1}$  (one channel).

The targets are finally observed under band 4 weather<sup>6</sup> in March and band 5 weather in August of 2015. In band 4

weather, the atmospheric zenith opacity at 225 GHz, as measured with the Water Vapour Monitor (measured in the direction in which the telescope is observing), or the CSO tau meter (measuring in a fixed direction), is between 0.12 and 0.20. In band 5 weather, the zenith opacity is between 0.20 and 0.32. The on-source integration time per scan was 400 s and one such scan took 13 minutes. The observation mode was “double beam switching”<sup>7</sup> over 60 arcsec (to both sides with respect to the source). The total integration time of each object is about two hours and eight hours for band 4 weather and band 5 weather, respectively. The data are calibrated by ORAC-DR (Hirst & Cavanagh 2005) data-reduction pipeline<sup>8</sup> using STARLINK software. In Table 2, columns 2–6 show details about the observations of the  $CO(J=2-1)$  emission line.

<sup>7</sup> <http://www.eaobservatory.org/jcmt/instrumentation/heterodyne/observing-modes/>

<sup>8</sup> <http://starlink.eao.hawaii.edu/devdocs/sun260.htx/sun260.html>

<sup>6</sup> <http://www.eaobservatory.org/jcmt/observing/weather-bands/>

**Table 1**  
Parameters of Low Surface Brightness Galaxies

Name	R.A. (J2000)	Decl. (J2000)	$V_{\text{He I}}$ ( $\text{km s}^{-1}$ )	$\mu_{\text{B}}(\text{obs})$ (mag arcsec $^{-2}$ )	$W_{50}^{\text{a}}$ ( $\text{km s}^{-1}$ )	$\log M_{\text{H I}}$ ( $M_{\odot}$ )	$D$ (Mpc)	Major-axis (arcsec)	$z$	$\text{NUV}_{\text{AB}}$ (mag)	$\tau_{\text{SDSS}}$ (mag)	$WJ^{\text{b}}$ (mag)	$W3^{\text{c}}$ (mag)
AGCf188845	08:01:13.02	+11:37:24.48	4935	23.056	79	8.99	72.5	54	0.0164	...	16.30	13.923	...
AGCf4528	08:40:58.60	+16:11:00.14	4288	22.900	88	9.40	63.6	66	0.0143	17.56	$\pm 0.02$	$\pm 0.044$	...
AGCf12212	22:50:30.26	+29:08:19.52	894	23.040	99	9.34	24.3	62	0.0029	$\pm 0.02$	$\pm 0.01$	$\pm 0.028$	...
AGCf110150	01:14:45.56	+27:08:11.10	3617	22.760	108	9.49	49.5	80	0.0120	17.52	$\pm 0.01$	...	...
AGCf102243	00:05:05.06	+23:58:14.09	6575	22.500	139	9.78	89.0	52	0.0219	$\pm 0.03$	$\pm 0.01$	...	...
AGCf12289	22:59:41.52	+24:04:29.77	10165	22.650	217	10.3	140.2	35	0.0339	...	$\pm 0.04$	$\pm 0.019$	$\pm 0.336$
AGCf102981	00:02:55.56	+28:16:38.78	4583	22.540	65	8.72	66.2	46	0.0152	...	$\pm 0.00$	$\pm 0.007$	$\pm 0.034$
AGCf102635	00:16:12.22	+24:50:59.04	9491	22.573	94	9.65	138.7	46	0.0316	18.34	$\pm 0.00$	$\pm 0.012$	$\pm 0.117$
NGC 7589	23:18:15.60	+00:15:40.00	8938	25.000 <sup>d</sup>	345	10.01	120.7	76	0.0298	$\pm 0.04$	$\pm 0.01$	$\pm 0.026$	$\pm 0.261$
										17.53	14.08	11.084	8.26
										$\pm 0.01$	$\pm 0.00$	$\pm 0.009$	$\pm 0.024$

**Notes.**

<sup>a</sup>  $W_{50}$  is the full width at half maximum (FWHM) of the H emission line.

<sup>b</sup>  $WJ$  is 3.4  $\mu\text{m}$  band of the *WISE*.

<sup>c</sup>  $W3$  is 12  $\mu\text{m}$  band of the *WISE*.

<sup>d</sup> For NGC 7589, its surface brightness is from de Vaucouleurs et al. (1991).

**Table 2**  
Observation Details

Name	Receiver	Weather Band	Frequency (GHZ)	Integration Time (hr)	Rms Noise (mk)	Facility	H $\alpha$ Filter <sup>a</sup> (Å)	Exp <sub>H<math>\alpha</math></sub> (s)	Exp <sub>Rband</sub> (s)
AGCNR188845	RxA3/JCMT	4	226.91	1.63	2.7	BFOSC/2.16	6660.0	1800	600
AGCNR4528	RxA3/JCMT	4	227.29	2.62	2.0	BFOSC/2.16	6660.0	1800	600
AGCNR12212	RxA3/JCMT	5	229.86	7.8	2.1	...	...	...	...
AGCNR110150	RxA3/JCMT	5	227.67	7.4	2.8	BFOSC/2.16	6660.0	1800	600
AGCNR102243	RxA3/JCMT	5	225.60	7.8	2.6	BFOSC/2.16	6710.0	1800	600
AGCNR12289	RxA3/JCMT	5	222.99	7.6	3.3	BFOSC/2.16	6760.0	1800	600
AGCNR102981	RxA3/JCMT	5	227.06	7.8	2.0	BFOSC/2.16	6660.0	1800	600
AGCNR102635	RxA3/JCMT	5	223.47	8.3	3.1	BFOSC/2.16	6760.0	1800	600
NGC 7589	RxA3/JCMT	5	223.87	7.8	2.1	...	...	...	...

**Note.**<sup>a</sup> The central wavelength of H $\alpha$  filter.

### 2.3. H $\alpha$ Images

The H $\alpha$  images of NGC 7589 and AGCNR12212 have been observed by van Zee (2000), Epinat et al. (2008), and Subramanian et al. (2016). The H $\alpha$  images of other seven LSBGs were observed by the 2.16 m telescope at Xinglong Observatory, administered by the National Astronomical Observatories, Chinese Academy of Sciences (NAOC). This facility houses the BAO Faint Object Spectrograph and Camera (BFOSC; Fan et al. 2016) with a  $1272 \times 1152$  E2V CCD. The field of view is about  $9.46$  arcmin  $\times$   $8.77$  arcmin. The pixel size is  $0''.475$  and the gain is  $1.08$  e/ADU. Each target was observed with a broadband R filter and one narrowband H $\alpha$  filter. The center wavelength of the R-band filter is  $6407$  Å and the full width at half maximum (FWHM) is  $1580$  Å. According to the different redshifts of objects, we employed H $\alpha$  filters with different central wavelengths of  $6660$  Å,  $6710$  Å, and  $6760$  Å and an FWHM of  $70$  Å. The exposure times are about  $600$  s and  $1800$  s for the R band and H $\alpha$  narrowbands, respectively.

The image reduction is performed by using IRAF software and the sky background subtraction applied the more accurate method by Zheng et al. (1999), Wu et al. (2002), and Du et al. (2015). The stellar continuum of each H $\alpha$  image is removed by subtracting the scaled R-band image. Finally, we measured the H $\alpha$  fluxes of these LSBGs, using the ellipse photometry of IRAF. In Table 2, columns 7–10 list the details of observations of H $\alpha$  images. AGCNR102981 is affected by light pollution from a nearby bright star.

## 3. Results and Analysis

### 3.1. H $_2$ Masses

To enhance signal-to-noise, we binned the CO( $J=2-1$ ) spectral channels. The final CO( $J=2-1$ ) spectral have been smoothed to  $15$  km s $^{-1}$  as shown in Figure 2. Apparently, None of nine targets are detected CO( $J=2-1$ ) content.

To estimate the molecular hydrogen masses, we adopted  $W_{50}$  as the linewidth. Here,  $W_{50}$  is the FWHM of H I emission line. The  $W_{50}$  of our targets is about  $65-345$  km s $^{-1}$ . The aperture efficiency  $\eta_a$  is  $0.61$  at  $225$  GHz, and the conversion from  $T_A$  in kelvin to flux density in Jansky is  $S(\text{Jy}) = 15.6 \times T_A(\text{K})/\eta_a$ , for JCMT. In this work, the  $T_A$  is replaced by the  $3\sigma/\sqrt{n}$ , where the  $\sigma$  is the rms noise at native resolution and  $n$  is the number of channels to smooth velocity resolution to  $15$  km s $^{-1}$ . Hence, flux densities in Jansky are calculated according to

equation:  $S_{\text{CO}(J=2-1)}(\text{Jy}) = 15.6 \times 3 \times \sigma/\sqrt{n}/\eta_a$ . Here we adopt the  $R_{21} = \text{CO}(J=2-1)/\text{CO}(J=1-0) = 0.7$  (Leroy et al. 2009; Schruba et al. 2012).

The CO-to-H $_2$  conversion equation is as follows.

$$M_{\text{H}_2} = \alpha_{\text{CO}} \times L_{\text{CO}} \quad (1)$$

$$L_{\text{CO}} = 3.25 \times 10^7 \times S'_{\text{CO}} \times \nu_{\text{obs}}^{-2} \times D^2 \times (1+z)^{-3}. \quad (2)$$

In Equation(1),  $M_{\text{H}_2}$  is molecular hydrogen mass in  $M_{\odot}$  and  $L_{\text{CO}}$  is CO luminosity in  $\text{K km s}^{-1} \text{pc}^2$ . In Equation(2),  $S'_{\text{CO}}$  is integrated CO flux density in  $\text{Jy km s}^{-1}$ . We adopt linewidth  $W_{50}$  and the resolution  $15$  km s $^{-1}$ , such as  $S'_{\text{CO}(J=1-0)} = S_{\text{CO}(J=1-0)} \times W_{50}/15$ .  $\nu_{\text{obs}}$  is observation frequency in GHz,  $D$  is distance in Mpc, and  $z$  is redshift.

In different environments, the  $X_{\text{CO}}$  factor is different. Considering that the conversion factor of CO-to-H $_2$  increases with decreasing metallicity,  $X_{\text{CO}}$  is chosen to be  $3.162 \times 10^{20} \text{ cm}^{-2}/(\text{K km s}^{-1})$  ( $X_{\text{CO}} = \alpha_{\text{CO}} \times 6.3 \times 10^{19} \text{ pc}^2 \text{ cm}^{-2} M_{\odot}^{-1}$ ,  $\alpha_{\text{CO}}$  simply is a mass-to-light ratio in  $M_{\odot} (\text{K km s}^{-1} \text{pc}^2)^{-1}$  Bolatto et al. 2013), which is also the same as previous works (Matthews & Gao 2001; Matthews et al. 2005). From Equation (1), we can calculate upper limits of molecular hydrogen masses per beam, which are about  $(0.68-31.6) \times 10^7 M_{\odot}$ .

To compare with previous works, we correct the beam size to the CO disk size of our LSBGs. We estimate the upper limits of total molecular hydrogen masses of our sample. The beam filling factors are defined as the ratios between the area of beam and the total area of the CO disk, which is generally half of the optical disk (Young & Knezek 1989), and listed in Table 3. The major-axis of optical disks are given by R-band images and listed in the Table 1. The size of NGC 7589 is from Lauberts & Valentijn (1989). The upper limits of total molecular hydrogen masses are about  $(1.2-82.4) \times 10^7 M_{\odot}$ , which are listed in Table 3. Since the H I disk is more extended in LSBGs, the CO disk may be larger than half of optical disk. The total molecular hydrogen masses may be underestimated in Table 3. In the following parts of this paper,  $M_{\text{H}_2}$  represents the total molecular hydrogen mass.

In Figure 3, we plot the  $M_{\text{H}_1}$  versus  $M_{\text{H}_2}$  including our sample and LSBGs from some previous works. We have calculated the average molecular mass with bin size in  $10^{0.5} M_{\odot}$ . The average of  $M_{\text{H}_2}$  of LSBGs is smaller than those in SF galaxies for a given H I mass. We can see that upper limits of  $M_{\text{H}_2}$  in our work are consistent with previous works. LSBGs are deficient of the molecular gas compared with these SF galaxies.

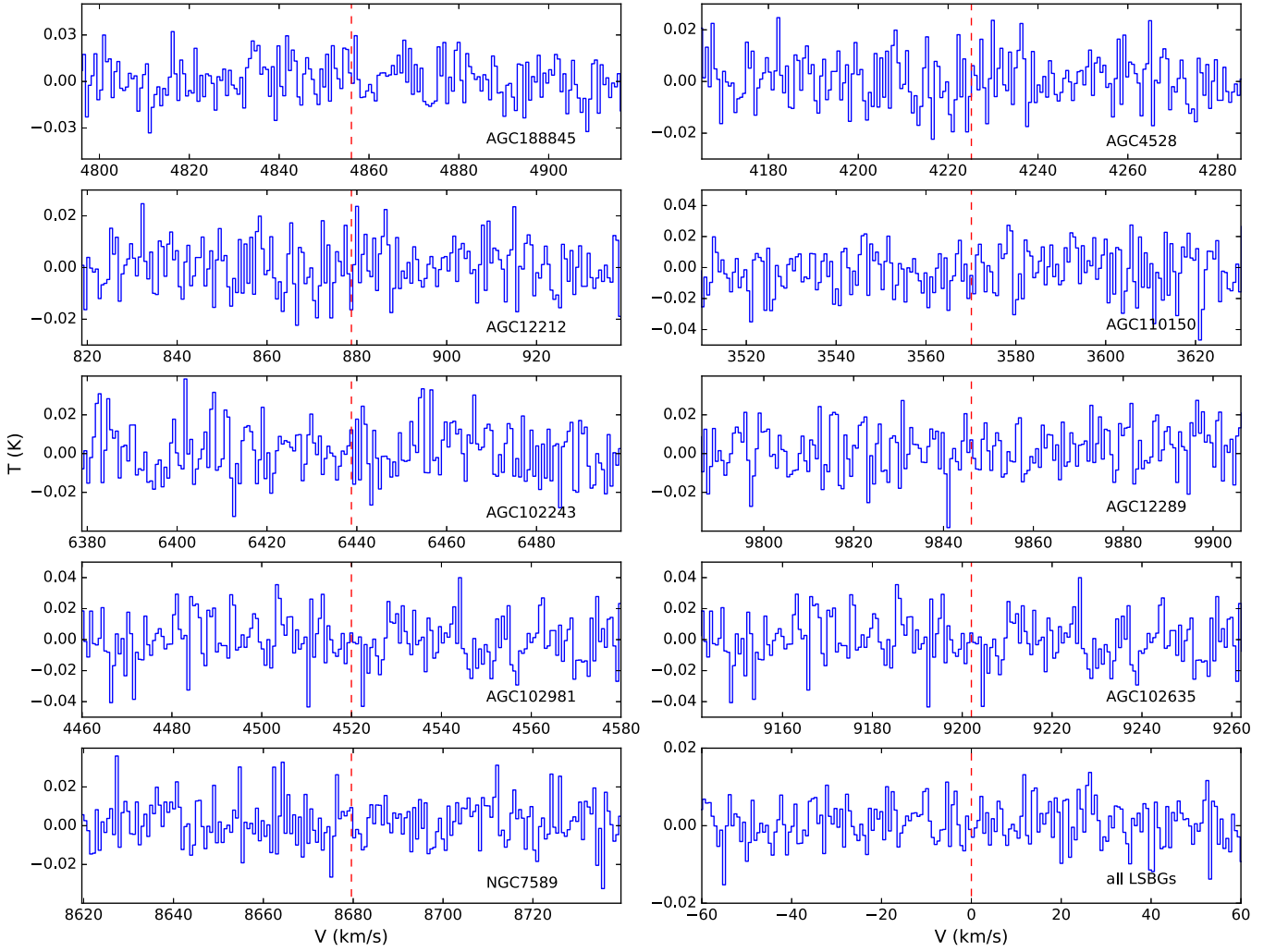


**Figure 2.** Nine individual and combined CO( $J = 2 - 1$ ) spectra of LSBGs. The red dashed line marks the position of the emission line of the redshifted CO( $J = 2 - 1$ ).

**Table 3**  
Upper limits of H<sub>2</sub> Masses in the Beam Size

Name	SFR <sub>H<math>\alpha</math></sub> ( $M_{\odot} \text{ yr}^{-1}$ )	log(SFE) <sub>H<math>\alpha</math></sub> ( $\text{yr}^{-1}$ )	SFR <sub>NUV</sub> ( $M_{\odot} \text{ yr}^{-1}$ )	log(SFE) <sub>NUV</sub> ( $\text{yr}^{-1}$ )	log $L_{\text{CO}}$ ( $\text{K km s}^{-1} \text{ pc}^2$ )	Beam Fill- ing Factor	log $M_{\text{H}_2\text{Total}}$ ( $M_{\odot}$ )	$M_{\text{H}_2\text{Total}}/M_{\text{H I}}$	log $L_{3.4}$ ( $L_{\odot}$ )	log $M_{*}$ ( $M_{\odot}$ )
AGCnr188845	0.097	-10.012	...	...	<6.71	1.35	<7.635	<0.044	7.316	8.154
AGCnr4528	0.079	-10.500	0.232	-10.037	<6.50	1.65	<7.643	<0.017	7.437	8.290
AGCnr12212 <sup>a</sup>	0.111	-10.300	...	...	<5.747	1.55	<7.612	<0.0201	...	...
	0.056	-10.599	...	...	...	...	...	...	...	...
AGCnr110150	0.108	-10.457	0.146	-10.327	<6.52	2.07	<7.827	<0.022	...	...
AGCnr102243	0.829	-9.865	...	...	<7.10	1.35	<8.017	<0.017	7.665	8.545
AGCnr12289 <sup>b</sup>	0.339	-10.776	...	...	<7.79	1.00	<8.615	<0.020	8.795	9.810
AGCnr102981 <sup>c</sup>	NAN	...	...	...	<6.411	1.76	<7.07	<0.018	7.760	8.651
AGCnr102635	0.367	-10.085	0.539	-9.930	<7.39	1.76	<8.336	<0.048	8.029	8.952
NGC 7589 <sup>d</sup>	0.173	-10.782	1.003	-10.018	<7.66	1.90	<8.960	<0.0806	8.894	9.922

**Notes.**

<sup>a</sup> For AGCnr12212, the two different SFR<sub>H $\alpha$</sub>  results are from the works of van Zee (2000) and Epinat et al. (2008). We did not derive its H $\alpha$  flux from our observation.

<sup>b</sup> The result with the observations of JCMT. The CO content of AGCnr12289 was detected by O’Neil et al. (2003) with the IRAM and the ratio of  $M_{\text{H}_2}/M_{\text{H I}}$  is 0.008.

<sup>c</sup> For AGCnr102981, we did not derive its H $\alpha$  flux from our observation.

<sup>d</sup> For NGC 7589, the SFR<sub>H $\alpha$</sub>  is calculated by SDSS spectra (Subramanian et al. 2016).

32 nearby gas-rich SF galaxies in Figure 3 are from Jiang et al. (2015) and observed with the Sub-millimeter Telescope. Their H I masses are from the ALFALFA catalog. These SF galaxies

are intermediate-mass galaxies ( $<10^{10} M_{\odot}$ ). The intermediate-mass galaxies were found to be more gas rich (Blanton & Moustakas 2009). These galaxies present the low-mass end of

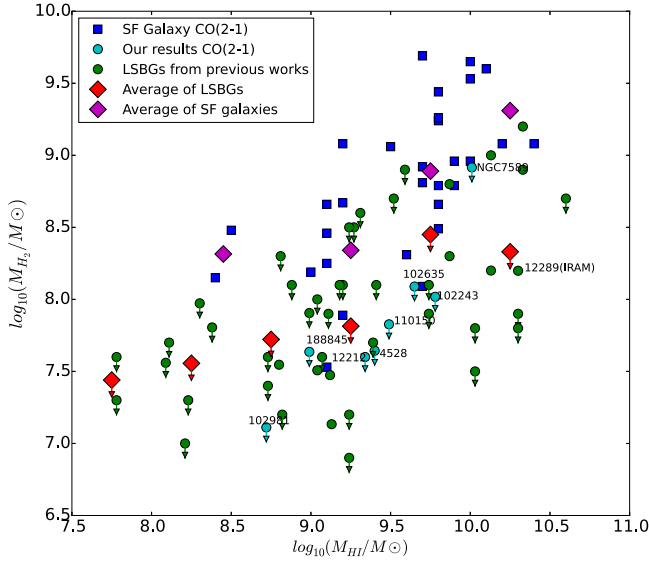


**Figure 3.** H I mass vs. H<sub>2</sub> mass. The cyan dots are LSBGs from this survey, the green dots are LSBGs from previous works (Schombert et al. 1990; de Blok & van der Hulst 1998a; Braine et al. 2000; O’Neil et al. 2000, 2003). Blue squares are SF galaxies from Jiang et al. (2015). The red and purple diamonds present the average molecular mass of LSBGs and SF galaxies, respectively. The arrows indicate the upper limits.

main-sequence SF galaxies. Both the molecular mass of our sample and the SF galaxies sample are calculated by the CO ( $J=2-1$ ) emission line, so the SF galaxies are selected as a comparison sample.

Some reasons could explain the lack of molecular gas in LSBGs. First, metallicity can affect the cooling efficiency of the interstellar medium (ISM), which may impact the formation of giant molecular clouds (GMCs). Second, dust grains where H<sub>2</sub> forms (Savage & Mathis 1979) can shield molecular gas from photodissociation. The low ISM densities make it hard for molecular clouds to form and be maintained.

The low metallicities and low ISM densities in LSBGs can make it either difficult to form H<sub>2</sub> or easy to destroy H<sub>2</sub>.

### 3.2. Star-formation Rates

We adopt H $\alpha$  luminosity to calculate the SFR of our sample. As the dust in LSBGs is usually less, few targets can be detected in the 22  $\mu\text{m}$  (*WISE W4*) band, so we ignore the dust extinction in our sample.

The SFR of AGCNR12212 has been found to be  $0.111 M_{\odot} \text{ yr}^{-1}$  in the work of van Zee (2000) and  $0.056 M_{\odot} \text{ yr}^{-1}$  in the work of Epinat et al. (2008). Six H $\alpha$  fluxes of LSBGs are available from our observation. We transform H $\alpha$  fluxes to luminosity using the relation:  $L = 4 \times \pi \times D^2 \times F$ , where  $D$  is distance in centimeters and  $F$  is H $\alpha$  flux in  $\text{erg s}^{-1} \text{ cm}^2$ . We employ the following equation to calculate SFR (Kennicutt 1998).

$$\text{SFR}_{\text{H}\alpha}(M_{\odot} \text{ yr}^{-1}) = 7.9 \times 10^{-42} \times L_{\text{H}\alpha} \text{ erg s}^{-1}. \quad (3)$$

The derived SFRs are from  $0.056$  to  $0.829 M_{\odot} \text{ yr}^{-1}$ .

We also use the NUV-band luminosity to calculate SFR of four sources (AGCNR4528, 110150, 102635, and NGC 7589), which have NUV data from *GALEX*. We adopt the following equation (Kennicutt 1998).

$$\text{SFR}_{\text{NUV}}(M_{\odot} \text{ yr}^{-1}) = 1.4 \times 10^{-28} \times L_{\nu}(\text{erg s}^{-1} \text{ Hz}^{-1}). \quad (4)$$

The NUV-based SFRs are  $0.146 \sim 1.003 M_{\odot} \text{ yr}^{-1}$ , which are systematically larger than those calculated from H $\alpha$  luminosity. The UV emission is also contaminated by older stars, so this would lead to deriving higher SFR from UV than that from the H $\alpha$ . All these values are listed in the Table 3.

In Figure 4, we show SFR versus HI mass for our sample and black lines connect the same target. We also show another sample of LSBGs in green dots from Boissier et al. (2008) whose SFRs are estimated by NUV luminosity. The figure shows an increase of the SFR with HI mass. SFR in LSBGs is about  $0.2 M_{\odot} \text{ yr}^{-1}$  in the model calculations of McGaugh & Bothun (1994) and  $0.17-0.36 M_{\odot} \text{ yr}^{-1}$  by H $\alpha$  (Burkholder et al. 2001), they are lower than that of SF galaxies. The low SFRs of our sample are consistent with previous results. The low SFR in LSBGs agrees with the low molecular hydrogen mass.

### 3.3. Star-formation Efficiency

SFE (Leroy et al. 2008) is the ratio of star-formation rate to total mass of gas ( $\text{SFE} = \text{SFR} / M_{\text{gas}}$ ).  $M_{\text{gas}}$  is the total gas mass that can be estimated by H<sub>2</sub> mass and HI mass ( $M_{\text{H}_2} + M_{\text{H I}}$ ).

The SFR and  $M_{\text{H}_2}$  of our sample have been calculated in Sections 3.1 and 3.2.  $M_{\text{H I}}$  is from the ALFALFA catalog listed in Table 2. Since  $M_{\text{H}_2}$  is far smaller than  $M_{\text{H I}}$ , we adopt  $M_{\text{H I}}$  to replace  $M_{\text{gas}}$ . SFE can be calculated by  $\text{SFR}_{\text{H}\alpha}$  and  $\text{SFR}_{\text{UV}}$ , respectively. SFEs of our LSBGs are  $(0.165 \sim 1.364) \times 10^{-10} \text{ yr}^{-1}$  by  $\text{SFR}_{\text{H}\alpha}$  and  $(0.471 \sim 1.174) \times 10^{-10} \text{ yr}^{-1}$  by  $\text{SFR}_{\text{UV}}$ , respectively. The results are shown in Table 3.

SFEs of LSBGs are lower than  $1.364 \times 10^{-10} \text{ yr}^{-1}$  and are far lower than  $5.25 \times 10^{-10} \text{ yr}^{-1}$  observed in normal spiral galaxies (Leroy et al. 2008). Generally, molecular gas is directly related to star formation, so SFE can reflect the efficiency of transforming the hydrogen atom to molecular hydrogen. Low SFE may hint that atomic hydrogen produces molecular hydrogen at a low speed. In short, the low SFR and SFE imply a lack of molecular hydrogen gas in LSBGs and this will be discussed in Section 4.

## 4. Discussion

### 4.1. Comment of Individual Galaxies

AGCNR12289 is a late-type spiral galaxy with a optical disk size of about  $35''$  and has a potential AGN/LINER core (Schombert 1998). There is a supernova (SN2002en) in AGCNR12289. O’Neil et al. (2003) has detected CO( $J=1-0$ ,  $J=2-1$ ) content in AGCNR12289 using the IRAM 30 m telescope. The  $M_{\text{H}_2}$  of AGCNR12289 is about  $15.8 \times 10^7 M_{\odot}$  using CO( $J=2-1$ ) observed by IRAM, which is lower than our upper limit of  $41.2 \times 10^7 M_{\odot}$ . The ratio of  $M_{\text{H}_2}/M_{\text{H I}}$  is 0.008 for AGCNR12289.

AGCNR188845, AGCNR102243, AGCNR102635, and AGCNR102981: For these galaxies, the optical sizes are about  $54''$ ,  $52''$ ,  $46''$ , and  $46''$ . From our calculations, the  $M_{\text{H}_2}/M_{\text{H I}}$  are lower than 0.044, 0.017, 0.048, and 0.018, respectively. The metallicity of AGCNR188845 is 0.01 and one-half of solar metallicity. AGCNR102981 is a typical late-type spiral galaxy and the spiral structures are shown in Figure 1.

AGCNR4528, AGCNR12212, and AGCNR110150: The optical sizes of these three galaxies are about  $66''$ ,  $62''$ , and  $80''$ , respectively, which indicate that JCMT’s beam size is not enough to cover their total CO content. The metallicity of AGCNR4528 is 0.02 and same to solar metallicity. The  $M_{\text{H}_2}/M_{\text{H I}}$  for these three LSBGs are lower than 0.018, 0.0201, and 0.022 respectively.

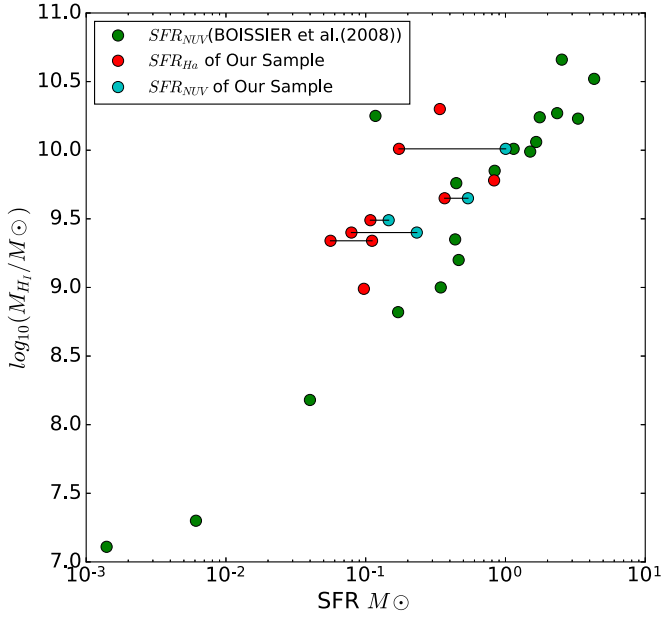


**Figure 4.** H I mass vs. SFR. The red dots are SFRs calculated by H $\alpha$  and the blue dots are SFRs calculated by NUV luminosity. The black line connects the same target. The green dots are the sample of LSBGs from Boissier et al. (2008).

*NGC 7589*: The optical size of *NGC 7589* is 76". It is a Seyfert-1 galaxy. The SFR from NUV band is  $1.003 M_{\odot} \text{ yr}^{-1}$  and its metallicity is 0.04 and twice the solar metallicity. There are some works investigating this galaxy. It is a typical giant LSBG and has type 1 XUV-disk galaxy (Boissier et al. 2008). The upper limit of  $M_{\text{H}_2}$  is  $8.25 \times 10^8 M_{\odot}$  and the ratio of  $M_{\text{H}_2}/M_{\text{H}_1}$  is lower than 0.081.

#### 4.2. $M_{\text{H}_2}$ versus $L_{12\mu\text{m}}$

The  $12 \mu\text{m}$  (*WISE W3*) band is an effective probe of star formation (Donoso et al. 2012) and has a good linear relationship with molecular hydrogen mass for SF galaxies (Jiang et al. 2015). In this section, we try to explore the relation between molecular gas and  $12 \mu\text{m}$  emission in LSBGs.

Five sources in our sample have  $12 \mu\text{m}$  emission data provided by the *WISE ALL-sky Survey*. Figure 5 shows  $L_{12\mu\text{m}}$  versus  $M_{\text{H}_2}$ . The blue line in Figure 5 is the relationship between  $M_{\text{H}_2}$  ( $\text{CO}_{J=2-1}$ ) and luminosity of  $12 \mu\text{m}$  for SF galaxies (Jiang et al. 2015).

AGCNR12289 and *NGC 7589* have higher luminosities of  $12 \mu\text{m}$  in Figure 5. AGCNR12289 has a potential AGN/LINER core and *NGC 7589* is a Seyfert-1 galaxy that may cause them to be different from other LSBGs in our sample. The LSBGs show low luminosities of  $12 \mu\text{m}$  and it may mean less dust in LSBGs. For SF galaxies, they always have larger  $12 \mu\text{m}$  luminosities compared with LSBGs.

#### 4.3. The Stellar Mass and Gas Content

Six LSBGs of our sample have  $3.4 \mu\text{m}$  (*WISE W1*) band data. Using the method in Wen et al. (2013) by following Equation (5), we adopt  $3.4 \mu\text{m}$  data to calculate the stellar mass:

$$\log_{10}(M_*/M_{\odot}) = (-0.040 \pm 0.001) + (1.120 \pm 0.001) \times \log_{10}(\nu L_{\nu}(3.4 \mu\text{m})/L_{\odot}). \quad (5)$$

As the redshifts of our sample are small, we ignore the  $k$ -correction. Their stellar masses are about  $(1.41\text{--}83.17) \times 10^8 M_{\odot}$ .

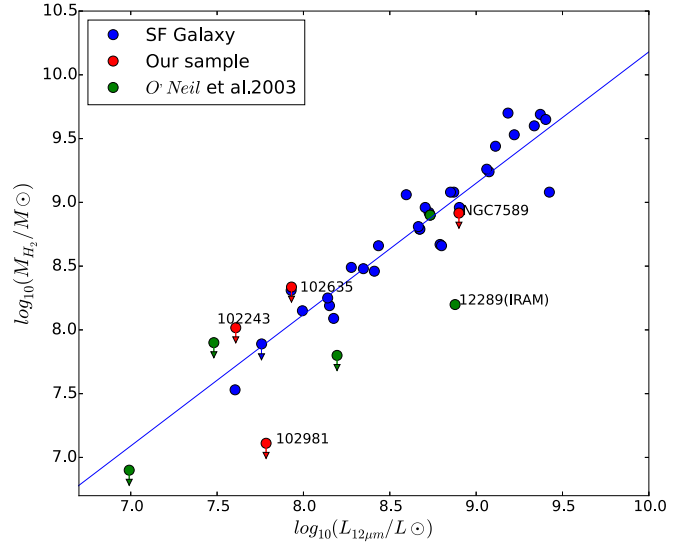


**Figure 5.** Luminosity of  $12 \mu\text{m}$  vs.  $M_{\text{H}_2}$ . The red dots are LSBGs from this work, green dots are from O'Neil et al. (2003) and the blue dots are SF galaxies from Jiang et al. (2015). The arrows indicate the upper limits.

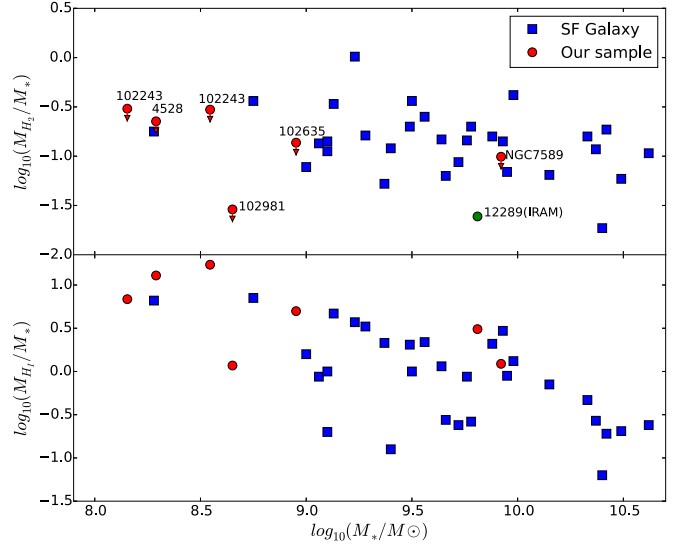


**Figure 6.** Stellar mass ( $M_*$ ) vs. the ratio of  $M_{\text{H}_2}/M_*$  (upper) and  $M_{\text{H}_1}/M_*$  (lower). The red dots are LSBGs from this work and the blue squares are SF galaxies (Jiang et al. 2015). The arrows indicate the upper limits.

LSBGs usually have low masses. The stellar masses of our sample are shown in Table 3.

The stellar masses of SF galaxies have a different relation with molecular gas and atomic gas. The ratios of  $M_{\text{H}_2}/M_*$  are almost constant (Jiang et al. 2015). We are more interested in the relation between stellar mass and gas content of LSBGs.

Figure 6 shows the relation between stellar mass  $M_*$  and gas content in SF galaxies and our LSBG sample. The  $M_{\text{H}_2}/M_*$  shows a flat trend within the considerable scatter and  $M_{\text{H}_1}/M_*$  shows an obvious decline with increasing stellar mass. It seems that the molecular gas fraction ( $M_{\text{H}_2}/M_*$ ) is similar in LSBGs and in SF galaxies, though our results provide upper limits, except for the AGCNR12289. Compared with SF galaxies, the stellar mass of our sample is mainly lower than  $10^9 M_{\odot}$ , excluding the two special galaxies (AGCNR12289

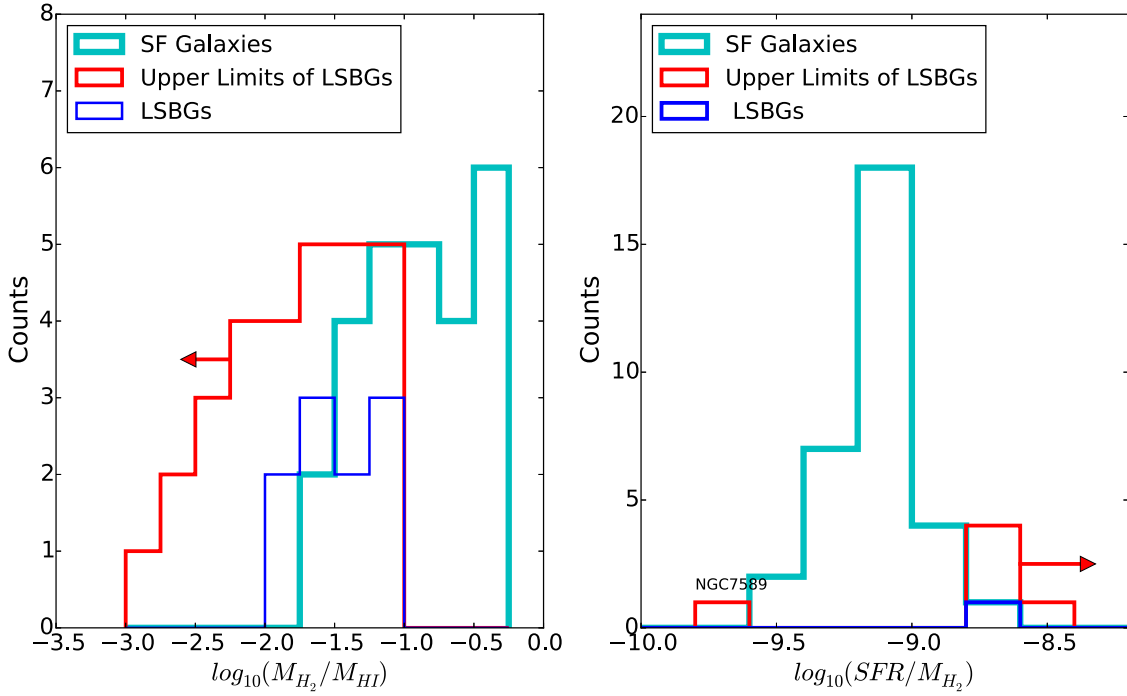


**Figure 7.** Left panel: the distribution of  $M_{\text{H}_2}/M_{\text{H}_1}$ . Right panel: the distribution of  $\text{SFR}/M_{\text{H}_2}$ . The red histogram represents upper limits of LSBGs and the blue histogram represents those detected molecular LSBGs. All LSBG data are from our sample and previous works (Schombert et al. 1990; de Blok & van der Hulst 1998a; Braine et al. 2000; O’Neil et al. 2000, 2003). The cyan histogram represents SF galaxies (Jiang et al. 2015). The arrows represent upper limits.

and NGC 7589). Stellar masses of AGC Nr12289 and NGC 7589 may be overestimated by the central AGN.

#### 4.4. $M_{\text{H}_2}/M_{\text{H}_1}$ and $\text{SFR}/M_{\text{H}_2}$

H I gas is the original material involved in star formation, and star formation is directly related to molecular gas. The  $M_{\text{H}_2}/M_{\text{H}_1}$  ratio should be different for different galaxies. The gas content could change along the main sequence of SF galaxies. Other factors, such as metallicity and environment could affect the ratio. Even for the same galaxy, its gas fraction would also change during its different evolutionary phase. In our nine LSBGs, the  $M_{\text{H}_2}/M_{\text{H}_1}$  ratios are less than 0.02. In typically brighter Sd–Sm spirals (Young & Knezek 1989), the  $M_{\text{H}_2}/M_{\text{H}_1}$  ratio is about 0.2.

In the Section 3.1, we have discussed the  $M_{\text{H}_1}$  and  $M_{\text{H}_2}$  in SF galaxies and LSBGs. The  $M_{\text{H}_2}$  in LSBGs is lower than that in SF galaxies. In this section, we compare  $M_{\text{H}_2}/M_{\text{H}_1}$  and  $\text{SFR}/M_{\text{H}_2}$  in those LSBGs and SF galaxies.

Figure 7 shows the distribution of  $M_{\text{H}_2}/M_{\text{H}_1}$  on the left and  $\text{SFR}/M_{\text{H}_2}$  on the right. In the right panel, NGC 7589 has completely different values of  $\text{SFR}/M_{\text{H}_2}$  from the other LSBGs because of AGN influence. Due to the dispersed distribution, the difference in  $\text{SFR}/M_{\text{H}_2}$  between SF galaxies and LSBGs is not quite obvious.

We can see that the ratios of  $M_{\text{H}_2}/M_{\text{H}_1}$  in LSBGs are less than those in SF galaxies. The rate of transforming atomic hydrogen to molecular hydrogen in LSBGs is lower than that in SF galaxies. In Section 3.1, we have also discussed the shortage of molecular gas in the special environment of LSBGs. However, CO is more easily photodissociated than  $\text{H}_2$  in a metal-poor environment (Wolfire et al. 2010; Shetty et al. 2011). Thus, the conversion factor of CO-to- $\text{H}_2$  is usually higher than that in SF galaxies. In this work, we adopt the factor of  $3.162 \times$

$10^{20} \text{ cm}^{-2}/(\text{K km s}^{-1})$  to be consistent with previous works. According to the work of Narayanan et al. (2012), the factor may be larger than  $3.16 \times 10^{20} \text{ cm}^{-2}/(\text{K km s}^{-1})$  and up to  $15 \times 10^{20} \text{ cm}^{-2}/(\text{K km s}^{-1})$ . So, the  $M_{\text{H}_2}$  of our sample may be underestimated. Although, due to the lack of detected CO content, it is still possible that  $M_{\text{H}_2}$  is underestimated in LSBGs.

## 5. Summary

We observed CO( $J=2-1$ ) emission lines in nine LSBGs with JCMT and  $\text{H}\alpha$  images with the 2.16 m telescope administered by NAOC. As no CO has been detected, only upper limits on the  $\text{H}_2$  masses are given. The upper limits of hydrogen molecular masses are about  $(1.2-82.4) \times 10^7 M_{\odot}$ . Their star-formation rates are about  $0.056-0.83 M_{\odot} \text{ yr}^{-1}$  and  $0.146-1.003 M_{\odot} \text{ yr}^{-1}$  estimated by  $\text{H}\alpha$  and NUV luminosities, respectively. The stellar masses are about  $(0.14-8.31) \times 10^9 M_{\odot}$ , estimated by the WISE3.4  $\mu\text{m}$  band. From our results, the  $M_{\text{H}_2}$  and stellar mass in LSBGs are lower than those in SF galaxies. Low SFRs in LSBGs may be related to low molecular hydrogen mass, which may indicate low productivity of atomic hydrogen transforming into molecular hydrogen. More direct detection of molecular gas of LSBG is the key to answering the question in the future.

We would like to thank the referee for helpful suggestions. We thank the Key Laboratory of Optical Astronomy and Xinglong Observing Station administered by NAOC for their help during observations. We also thank the ALFALFA team for providing the  $\alpha.40$  catalog, and the WISE team and GALEX team for their wonderful released data. We thank Dr. Xianzhong Zheng for given suggestions.







This project is supported by the National Natural Science Foundation of China (grant Nos. 11403037, 11733006,



11173030, 11225316, 11503013, 11403061, U1531245, and 11303038); This project is also supported by the Strategic Priority Research Program, “The Emergence of Cosmological Structures” of the Chinese Academy of Sciences (Grant No. XDB09000000) and the China Ministry of Science and Technology under the State Key Development Program for Basic Research (Grant Nos. 2012CB821803, 2014CB845705). This work is also sponsored in part by the Chinese Academy of Sciences (CAS), through a grant to the CAS South America Center for Astronomy (CASSACA) in Santiago, Chile.

The James Clerk Maxwell Telescope is operated by the East Asian Observatory on behalf of the National Astronomical Observatories of China and the Chinese Academy of Sciences, the National Astronomical Observatory of Japan, Academia Sinica Institute of Astronomy and Astrophysics, the Korea Astronomy and Space Science Institute, with additional funding support from the Science and Technology Facilities Council of the United Kingdom and participating universities in the United Kingdom and Canada. Our JCMT project ID is M15BI057.

### ORCID iDs

Tian-Wen Cao  <https://orcid.org/0000-0002-1335-6212>  
 Wei Du  <https://orcid.org/0000-0003-4546-8216>  
 Jan Wouterloot  <https://orcid.org/0000-0002-4694-6905>  
 Harriet Parsons  <https://orcid.org/0000-0002-6327-3423>  
 Yi-Nan Zhu  <https://orcid.org/0000-0002-2798-2783>  
 Chao-Jian Wu  <https://orcid.org/0000-0003-3514-6619>  
 Zhi-Min Zhou  <https://orcid.org/0000-0002-4135-0977>

### References

Blanton, M. R., & Moustakas, J. 2009, *ARA&A*, 47, 159  
 Boissier, S., Gil de Paz, A., & Boselli, A. 2008, *ApJ*, 681, 244  
 Bolatto, A. D., Wolfire, M., & Leroy, A. K. 2013, *ARA&A*, 51, 207  
 Braine, J., Herpin, F., & Radford, S. J. E. 2000, *A&A*, 358, 494  
 Burkholder, V., Impey, C., & Sprayberry, D. 2001, *AJ*, 122, 2318  
 Das, M., Boone, F., & Viallefond, F. 2010, *A&A*, 523, A63  
 Das, M., Kantharia, N., Ramya, S., et al. 2007, *MNRAS*, 379, 11  
 de Blok, W. J. G., McGaugh, S. S., & van der Hulst, J. M. 1996, *MNRAS*, 283, 18  
 de Blok, W. J. G., & van der Hulst, J. M. 1998a, *A&A*, 335, 421  
 de Blok, W. J. G., & van der Hulst, J. M. 1998b, *A&A*, 336, 49  
 de Blok, W. J. G., van der Hulst, J. M., & Bothun, G. D. 1995, *MNRAS*, 274, 235  
 de Vaucouleurs, G., de Vaucouleurs, A., Corwin, H. G., Jr., et al. 1991, in *Third Reference Catalogue of Bright Galaxies. Volume I: Explanations and*

*References. Volume II: Data for Galaxies Between 0h and 12h. Volume III: Data for Galaxies Between 12h and 24h* (New York: Springer)  
 Donoso, E., Yan, L., Tsai, C., et al. 2012, *ApJ*, 748, 80  
 Du, W., Wu, H., Lam, M. I., et al. 2015, *AJ*, 149, 199  
 Epinat, B., Amram, P., & Marcelin, M. 2008, *MNRAS*, 390, 466  
 Fan, Z., Wang, H., & Jiang, X. 2016, *PASP*, 128, 115005  
 Gerritsen, J. P. E., & de Blok, W. J. G. 1999, *A&A*, 342, 655  
 Giovanelli, R., Haynes, M. P., & Kent, B. R. 2005, *AJ*, 130, 2598  
 Haynes, M. P., Giovanelli, R., & Martin, A. M. 2011, *AJ*, 142, 170  
 Hirst, P., & Cavanagh, B. 2005, *StaUN*, 236  
 Impey, C., & Bothun, G. 1997, *ARA&A*, 35, 267  
 Jiang, X.-J., Wang, Z., Gu, Q., Wang, J., & Zhang, Z.-Y. 2015, *ApJ*, 799, 92  
 Jimenez, R., Padoan, P., Matteucci, F., & Heavens, A. F. 1998, *MNRAS*, 299, 123  
 Kennicutt, R. C., Jr. 1998, *ARA&A*, 36, 189  
 Knezek, P. M. 1993, PhD thesis, Massachusetts Univ., Amherst  
 Laubert, A., & Valentijn, E. A. 1989, *The Surface Photometry Catalogue of the ESO-Uppsala Galaxies* (Garching: ESO)  
 Leroy, A. K., Walter, F., & Bigiel, F. 2009, *AJ*, 137, 4670  
 Leroy, A. K., Walter, F., & Brinks, E. 2008, *AJ*, 136, 2782  
 Matthews, L. D., & Gao, Y. 2001, *ApJL*, 549, L191  
 Matthews, L. D., Gao, Y., Uson, J. M., & Combes, F. 2005, *AJ*, 129, 1849  
 Matthews, L. D., van Driel, W., & Monnier-Ragaigne, D. 2001, *A&A*, 365, 1  
 Matthews, L. D., & Wood, K. 2001, *ApJ*, 548, 150  
 McGaugh, S. S. 1994, *ApJ*, 426, 135  
 McGaugh, S. S., & Bothun, G. D. 1994, *AJ*, 107, 530  
 McGaugh, S. S., & de Blok, W. J. G. 1997, *ApJ*, 481, 689  
 Narayanan, D., Krumholz, M. R., Ostriker, E. C., & Hernquist, L. 2012, *MNRAS*, 421, 3127  
 O’Neil, K., Bothun, G., van Driel, W., & Monnier Ragaigne, D. 2004, *A&A*, 428, 823  
 O’Neil, K., Hofner, P., & Schinnerer, E. 2000, *ApJL*, 545, L99  
 O’Neil, K., Schinnerer, E., & Hofner, P. 2003, *ApJ*, 588, 230  
 Peebles, P. J. E. 2001, *ApJ*, 557, 495  
 Pickering, T. E., Impey, C. D., van Gorkom, J. H., & Bothun, G. D. 1997, *AJ*, 114, 1858  
 Pustilnik, S. A., Martin, J.-M., Tepliakova, A. L., & Kniazev, A. Y. 2011, *MNRAS*, 417, 1335  
 Savage, B. D., & Mathis, J. S. 1979, *ARA&A*, 17, 73  
 Schombert, J. 1998, *AJ*, 116, 1650  
 Schombert, J. M., Bothun, G. D., Impey, C. D., & Mundy, L. G. 1990, *AJ*, 100, 1523  
 Schrubba, A., Leroy, A. K., & Walter, F. 2012, *AJ*, 143, 138  
 Shetty, R., Glover, S. C., Dullemond, C. P., & Klessen, R. S. 2011, *MNRAS*, 412, 1686  
 Subramanian, S., Ramya, S., Das, M., et al. 2016, *MNRAS*, 455, 3148  
 van der Hulst, J. M., Skillman, E. D., Smith, T. R., et al. 1993, *AJ*, 106, 548  
 van Zee, L. 2000, *AJ*, 119, 2757  
 Wen, X.-Q., Wu, H., & Zhu, Y.-N. 2013, *MNRAS*, 433, 2946  
 Wolfire, M. G., Hollenbach, D., & McKee, C. F. 2010, *ApJ*, 716, 1191  
 Wu, H., Burstein, D., & Deng, Z. 2002, *AJ*, 123, 1364  
 Wyder, T. K., Martin, D. C., & Barlow, T. A. 2009, *ApJ*, 696, 1834  
 Young, J. S., & Knezek, P. M. 1989, *ApJL*, 347, L55  
 Zheng, Z., Shang, Z., & Su, H. 1999, *AJ*, 117, 2757